Climate Dynamics
https://doi.org/10.1007/s00382-020-05187-5

Effect of spring soil moisture over the Indo-China Peninsula on the following summer extreme precipitation events over the Yangtze River basin

Chujie Gao[1] · **Gen Li**[1,2,3] · **Bei Xu**[4,5] · **Xinyu Li**[1]

Received: 11 November 2019 / Accepted: 20 February 2020
© Springer-Verlag GmbH Germany, part of Springer Nature 2020

Abstract
Extreme precipitation events (EPEs) over the Yangtze River basin (YRB) exert widespread impacts on regional ecological environment and people's life. Using observed precipitation, atmospheric reanalysis, and land assimilation datasets, the present study explores the relationship between the summer EPEs over the YRB and the Meiyu front and their possible linkages with the preceding spring soil moisture anomalies over the Indo-China Peninsula (ICP). The analyses show that both the frequency and intensity of summer EPEs over the YRB are closely associated with the mean intensity of the Meiyu front, which exhibits a significant negative correlation with the soil moisture anomalies in the preceding spring over the ICP. An abnormally drier soil over the ICP in spring would evidently raise air temperature by suppressing local evapotranspiration, and vice versa. Owing to a strong memory of the ICP soil moisture, the persistent anomalous heating would elevate local geopotential height in summer, inducing an excessive westward extension of the Western Pacific subtropical high. Accordingly, a strengthened southwesterly wind at the lower troposphere brings abundant warm–wet air to the YRB, intensifying the mean Meiyu front. This is also verified by the diagnosis of vertical motion (omega) equation. As a result, the risk of summer EPEs (both the frequency and intensity) over the YRB would increase (decrease) with an abnormally drier (wetter) ICP soil during the preceding spring. For the summer EPEs over the YRB, our results suggest that the spring ICP soil moisture can be used as an important seasonal predictor.

Keywords Yangtze River basin · Extreme precipitation events · Soil moisture · Meiyu front · East Asian summer monsoon · Indo-China Peninsula

1 Introduction

The Yangtze River basin (YRB) is one of the most densely populated areas with a high degree of socioeconomic development in China (e.g., Lu 2004; Wen et al. 2007) and is thus vulnerable to extreme precipitation events (EPEs; Zhai et al. 2005; Jiang et al. 2010; Guan et al. 2011; Wang and Yan 2011). For instance, a devastating flood induced by local EPEs occurred over the YRB during the summer of 1998, causing more than 30 billion dollars in direct economic losses and more than 3000 deaths (Huang et al. 1998). Therefore, it is crucial to investigate the nature and causes of summer EPEs over the YRB.

The YRB summer precipitation is closely associated with the East Asian monsoon advancement and intensity (Ding 1992; Huang et al. 2003; Ding and Chan 2005). The Meiyu (known as plum rain in China), as a part of the East Asian summer monsoon, contributes most of the summer rainfall

✉ Gen Li
ligen@hhu.edu.cn

[1] College of Oceanography, Hohai University, Nanjing, China

[2] Southern Marine Science and Engineering Guangdong Laboratory (Zhuhai), Zhuhai, China

[3] Key Laboratory of Coastal Disaster and Defence (Hohai University), Ministry of Education, Nanjing, China

[4] Zhejiang Early Warning Center, Zhejiang Meteorological Bureau, Hangzhou, China

[5] Key Laboratory of Meteorological Disaster, Ministry of Education/International Joint Research Laboratory of Climate and Environment Change, Collaborative Innovation Center on Forecast and Evaluation of Meteorological Disasters, Nanjing University of Information Science and Technology, Nanjing, China

Published online: 27 March 2020

over the YRB (Ding 1992; Wang and Linho 2002; He et al. 2007). During the Meiyu period, a zonal rainband is nearly immobile over the YRB (Sampe and Xie 2010; Cen et al. 2015) and precipitation extremes occur frequently, inducing local flood disasters (Ninomiya and Shibagaki 2007). For example, the 1998 summer flood is known for its occurrence with the second Meiyu period (Zhou et al. 2005).

The Meiyu rainband is accompanied by a typical frontal structure in the lower troposphere called Meiyu front, which can be featured by a sharp gradient in equivalent potential temperature (Luo and Chen 2015; Li and Lu 2017). In summer, warm–wet air transported by the southwesterly monsoon passes over the southern China against the cold–dry air mass held over the north, forming the quasi-stationary Meiyu front and feeding the Meiyu rainband over the YRB. The abundant moisture and upward motion ahead of the Meiyu front provide the favorable conditions for intense precipitation (Sampe and Xie 2010; Luo and Chen 2015). The Meiyu system presents multi-scale features, from daily to weekly and meso-scale to large-scale (Ding et al. 2007). Previous studies (Li and Lu 2017; Gao et al. 2019) suggested that the interannual variability of the Meiyu front can exert a significant effect on that of summer mean precipitation over the YRB. In particular, the present study further finds that both the frequency and intensity of summer EPEs over the YRB are also closely associated with the mean intensity of the Meiyu front.

As a complex coupling system, the East Asian summer monsoon is evidently affected by the land surface thermal conditions (Hsu and Liu 2003; Huang et al. 2003; Wu et al. 2007; Zuo et al. 2012). Soil moisture, one of the most important climate factors on land, is tightly related to the local thermal state (Seneviratne et al. 2010; Bellucci et al. 2015). Its variation, especially in semi-arid regions, would cause evident climatic effects under climate change (Huang et al. 2015, 2016, 2017). Over the monsoonal region, the local thermal feedbacks of soil moisture would significantly adjust the large-scale atmospheric circulation, and in turn affects remote monsoonal precipitation (Douville et al. 2001; Douville 2002). Some previous studies suggested that the East Asian summer monsoon can be affected by the soil moisture anomalies in the pre-monsoon season (Liang and Chen 2010; Zhan and Lin 2011; Meng et al. 2014). For instance, based on the numerical experiments, Zuo and Zhang (2016) found that an abnormally lower soil moisture in spring over the Yangtze River to North China could increase land surface temperature and result in a increased land–sea temperature gradient, enhancing the summer monsoon. Liu et al. (2017) also revealed that spring soil moisture over the eastern China exerts evident effects on the monsoonal circulation and the YRB precipitation during the summer time.

Indo-China Peninsula (ICP) is located in the upper reaches of the southwesterly monsoonal wind flow. Numerical experiments have demonstrated that the ICP are indispensable for the East Asian summer monsoon (Chen and Chen 1991; Jin et al. 2006a). Jin et al. (2006b) suggested that the thermal contrast between the ICP and western Pacific is crucial in the monsoon formation. Zhang and Qian (2002) pointed out that an enhanced southwesterly monsoonal wind is associated with the stronger gradients of the horizontal temperature and geopotential height, which are induced by a continuous sensible heating over the ICP. Thus, the ICP land thermal condition might exert obvious impacts on the East Asian summer monsoon. Recently, Ma et al. (2018) found that the soil moisture over the ICP plays a key role in the monsoon system owing to its strong influence on local thermal states. Besides, Yang et al. (2019) and Gao et al. (2019) have shown that spring soil moisture over the ICP can be used as a seasonal predictor of the YRB summer climate. However, linkages between the ICP soil moisture anomalies in spring and the YRB precipitation extremes in the following summer remain unclear.

The present study explores the summer (June, July, and August) EPEs over the YRB and their relationship with the preceding spring (March, April, and May) soil moisture anomalies over the ICP. Our analyses show that both the frequency and intensity of summer EPEs over the YRB are closely associated with the mean intensity of summer Meiyu front. Furthermore, the Meiyu front intensity exhibits a significant negative correlation with soil moisture anomalies in the preceding spring over the ICP. To be specific, an abnormal surface heating induced by a too dry soil over the ICP in spring can sustain to summer, contributing to an excessive westward extension of the Western Pacific subtropical high (WPSH). The associated stronger southwesterly wind brings abundant warm–wet air to the YRB, feeding the Meiyu front and EPEs over the YRB. Our results provide an important source of seasonal predictability for the YRB summer extreme climate that can benefit local economic development and people's livelihood.

The rest of this paper is arranged as follows. Section 2 introduces the datasets and methods. In Sect. 3, we examine the characteristics of summer EPEs over the YRB and their relationship with the Meiyu front. Section 4 explores the processes of the ICP soil moisture in spring affecting the Meiyu front and the YRB EPEs in summer. Section 5 contains a summary with discussion.

2 Data and methods

The gridded (0.5° × 0.5°) dataset of daily observational precipitation is provided by the China Meteorological Administration and available online at http://data.cma.cn/data/cdcdetail/dataCode/SURF_CLI_CHN_PRE_DAY_GRID_0.5.html, which is interpolated by the data collected

from more than 2000 stations over the entire mainland of China and covers the period of 1961–2014 (Xu et al. 2009; Wu and Gao 2013). We also examine the Japanese 55-year reanalysis dataset (JRA-55) from the Japan Meteorological Agency, including monthly geopotential height, wind, humidity, and temperature fields (Kobayashi et al. 2015). The horizontal resolution and the time span of this dataset are 1.25° × 1.25° and 1958 to present, respectively. The monthly sea surface temperature (SST) data with a resolution of 1° × 1° during 1870 to present are from the Hadley Center Sea Ice and Sea Surface Temperature dataset (Rayner et al. 2003).

In addition, a long-term soil moisture dataset (1° × 1°) provided by the Global Land Data Assimilation System (GLDAS) V2.0 is adopted in our study, which spans from 1948 to 2010 (Rodell et al. 2004). The products of GLDAS 2.0 are produced by the National Centers for Environmental Prediction/Oregon State University/Air Force/Hydrologic Research Laboratory (NOAH) land surface model (Ek et al. 2003) with the meteorological forcing datasets developed by Princeton University (Sheffield et al. 2006). The GLDAS dataset has been widely used in the researches related to land processes over East Asia (Wu and Zhang 2013; Cheng et al. 2015; Cheng and Huang 2016). There are four soil layers in the dataset, i.e., 0–10 cm, 10–40 cm, 40–100 cm and 100–200 cm. The top layer soil directly provides feedbacks on atmosphere (Zuo and Zhang 2007; Dirmeyer 2011), and thus only the soil moisture in the first layer (0–10 cm) is here utilized.

The present study period is 1961–2010. For double checking our data reliabilities, we further adopt ERA-interim reanalysis dataset (including 7 cm soil moisture, surface temperature, and geopotential height fields with a resolution of 1° × 1° for the period of 1979–2010) provided by the European Centre for Medium-Range Weather Forecasts (ECMWF), which is believed to be well capturing the interannual variabilities of observed soil moisture and atmospheric states over Asia (Zuo and Zhang 2007; Gao et al. 2018). Moreover, a monthly global observed precipitation dataset (0.5° × 0.5°) from the Climatic Research Unit (CRU) at the University of East Anglia is used to verify the relationship between spring soil moisture over the ICP and summer EPEs over the YRB for the period including the recent 8 years (1961–2018).

In this study, the threshold of EPEs is set at 50 mm day^{-1}, which is used to denote intense precipitation enough to trigger floods and affect human activities by China operational meteorological services. Besides, according to Chen and Zhai (2013), in the warm season, the precipitation of 50 mm day^{-1} exceeds the 95th percentile of daily precipitation at most (90%) stations of China. Over the YRB, 50 mm day^{-1} in summer is generally over the 96th percentile based on our calculation (figure not shown). Therefore, the number of EPEs is defined as the number of days with precipitation amount meeting or exceeding 50 mm, and the intensity of EPEs is defined as averaged daily precipitation amount of all events for each summer.

Specifically, the equation for calculating water vapor flux is as follows:

$$Q = \frac{1}{g}\int_{Pt}^{Ps} \nabla \cdot (q\vec{V})dP, \tag{1}$$

where g is gravitational acceleration; q is specific humidity; $\vec{V}$ is horizontal wind velocity; and Ps and Pt are the surface and top air pressures. Water vapor is negligible in the levels above 300 hPa, and thus we only integrated from 300 to 1000 hPa. $Q > 0$ denotes the divergence of the flux.

Generally, precipitation extremes are associated with abnormal upward movements in the troposphere. Thus, we employ the omega equation to diagnose the vertical motion. The equation is as follows:

$$\sigma\left(\nabla^2 + \frac{f_0^2}{\sigma}\frac{\partial^2}{\partial p}\right)\omega = f_0\frac{\partial}{\partial p}\left[V_g \cdot \nabla\left(\frac{1}{f_0}\nabla^2\phi + f\right)\right] + \nabla^2\left[V_g \cdot \nabla\left(-\frac{\partial\phi}{\partial p}\right)\right] - \frac{k}{p}\nabla^2 J, \tag{2}$$

where each symbol has its conventional meaning in meteorology. For the detailed information, please see Holton (2004). The left term (referred as term A) of Eq. (2) is proportional to $-\omega$ (or w). The other three terms on the right are physical processes contributing to the vertical motion: the vertical gradient of absolute vorticity advection (referred as term B), temperature advection (referred as term C), and diabatic heating (referred as term D). Generally speaking, the term D is a relatively small term (Feng et al. 2014), thus only the term B and term C (adiabatic processes) are considered in this study. According to Eq. (2), a positive vertical gradient of absolute vorticity advection or a warm temperature advection is conductive to forming and maintaining the ascent.

The calculation of removing the SST anomaly signals is as the following equation:

$$V = V^* - S \times \mathrm{cov}(V^*, S)/\mathrm{var}(S), \tag{3}$$

where V^* is a given variable, V is the variable after removing the SST signal, S is the regional mean of SST in a key region, cov (V^*, S) is the covariance between the variable and the SST anomalies, and var (S) is the variance of the SST anomaly.

3 Summer precipitation over the YRB and the Meiyu front

3.1 Summer mean precipitation and its relationship with the Meiyu front

Figure 1 illustrates the climatic state of summer precipitation over the Eastern China. In general, the precipitation decreases from south to north (Fig. 1a). Over the Southern coastal region, the summer precipitation reaches more than 8 mm day^{-1}. The YRB is the secondary center with abundant precipitation by more than 6 mm day^{-1}. For the inter-annual standard deviation, the Southern China and the YRB exhibit relatively large values of more than 1.5 mm day^{-1} and 2.1 mm day^{-1}, respectively (Fig. 1b). Particularly, the proportion of the inter-annual standard deviation of summer precipitation in the summer mean precipitation over the YRB is even higher than that over the South China, up to 30–40% (Fig. 1c). This means that summer precipitation over the YRB exhibits a large inter-annual variability.

We calculated the annual cycle of regional precipitation averaged over the YRB (106° E–119° E and 28° N–33° N, Gao et al. 2019). Precipitation rapidly increases in warm season, and it reaches the peak in summer (figure not shown). Specifically, the local summer precipitation accounts for about 48% of the total annual precipitation. Such strong summer precipitation over the YRB is largely due to the quasi-stationary Meiyu front. The climatic states of summer equivalent potential temperature (θe) and water vapor flux are demonstrated in Fig. 2. As the southwesterly wind prevails over southern China, the warm and wet air is transported to the YRB against the cold and dry air held in the north. Therefore, a relatively higher θe dominates the southern China, leading to a large meridional θe gradient ($-$ dθe/dy) across the YRB (Fig. 2a), which is a widely used feature of the Meiyu front (Li and Lu 2017, 2018). Meanwhile, the moisture converges over the YRB, accompanied by an ascending motion in the middle troposphere (Fig. 2b), which are favorable for the precipitation. The cross-section of the correlation of the vertical velocity averaged over 106° E–119° E with the mean intensity of the Meiyu front (θe gradient over the YRB) exhibits a frontal structure more intuitively (Fig. 3a). When the Meiyu front is abnormally stronger, the YRB is dominated by an abnormally enhanced upward motion, which slopes northward with the height. Figure 3b shows the relationship between the summer mean precipitation over the YRB and the Meiyu front. Indeed, the summer mean precipitation is closely associated with the

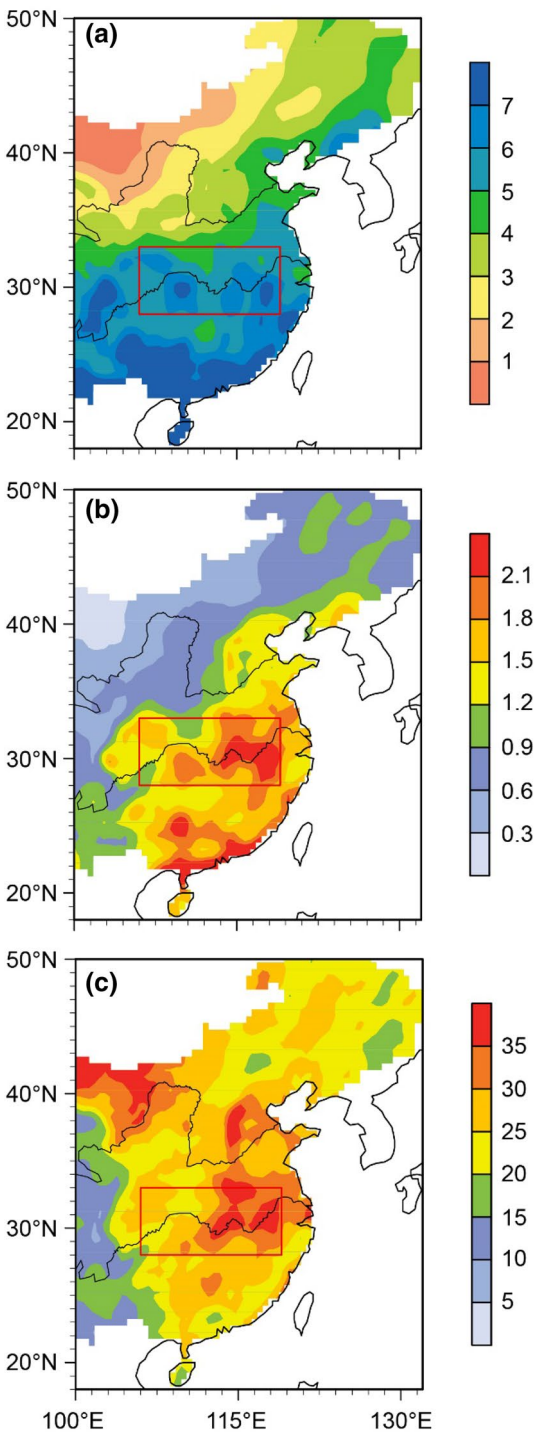

Fig. 1 **a** Climatology and **b** standard deviation of summer precipitation (units: mm day^{-1}) during 1961–2010. **c** Proportion of the summer precipitation standard deviation in the summer mean precipitation (units: %). Red box areas denote the Yangtze River basin (YRB)

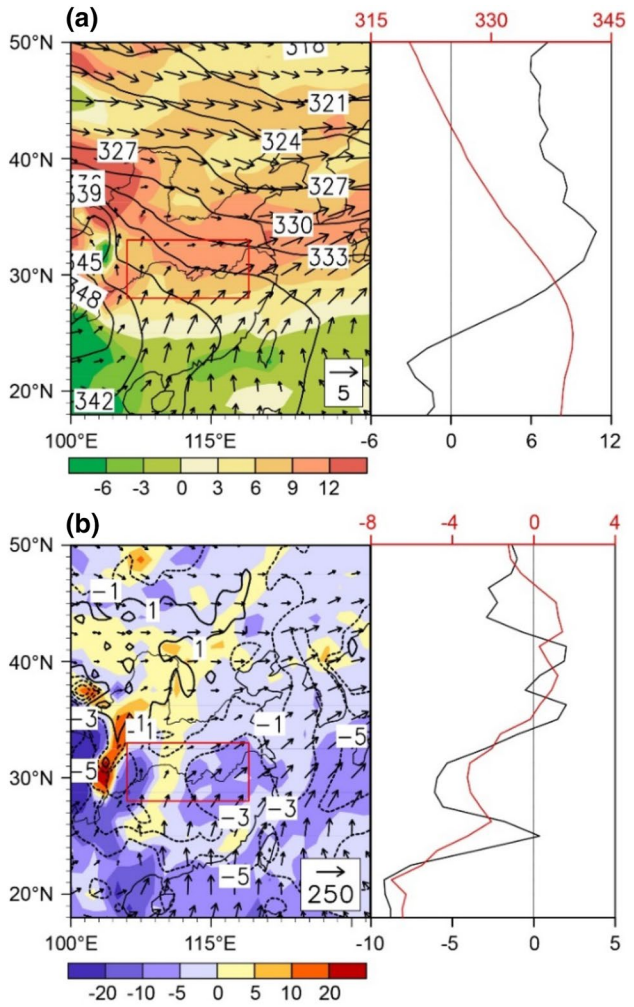

Fig. 2 **a** Summer means of the 700 hPa wind (arrows, units: m s^{-1}), equivalent potential temperature (contours, θe, units: K) and northward θe gradient (colors, $-$ dθe/dy, units: 1e^{-6} K m^{-1}) during 1961–2010. The right-hand panel shows the corresponding meridional θe (red line) and $-$ dθe/dy (black line) averaged over 106° E–119° E. **b** Summer means of the water vapor flux (arrows, units: kg m^{-1} s^{-1}) and its divergence (colors, units: 1e^{5} kg m^{-2} s^{-1}) integrated from 300 to 1000 hPa, and vertical velocity (contours, units: 1e^{-2} Pa s^{-1}) at 500 hPa during 1961–2010. The right-hand panel shows the corresponding meridional vertical velocity (red line) and water vapor divergence (black line), in which the negative values denote the upward motion and water vapor convergence, respectively

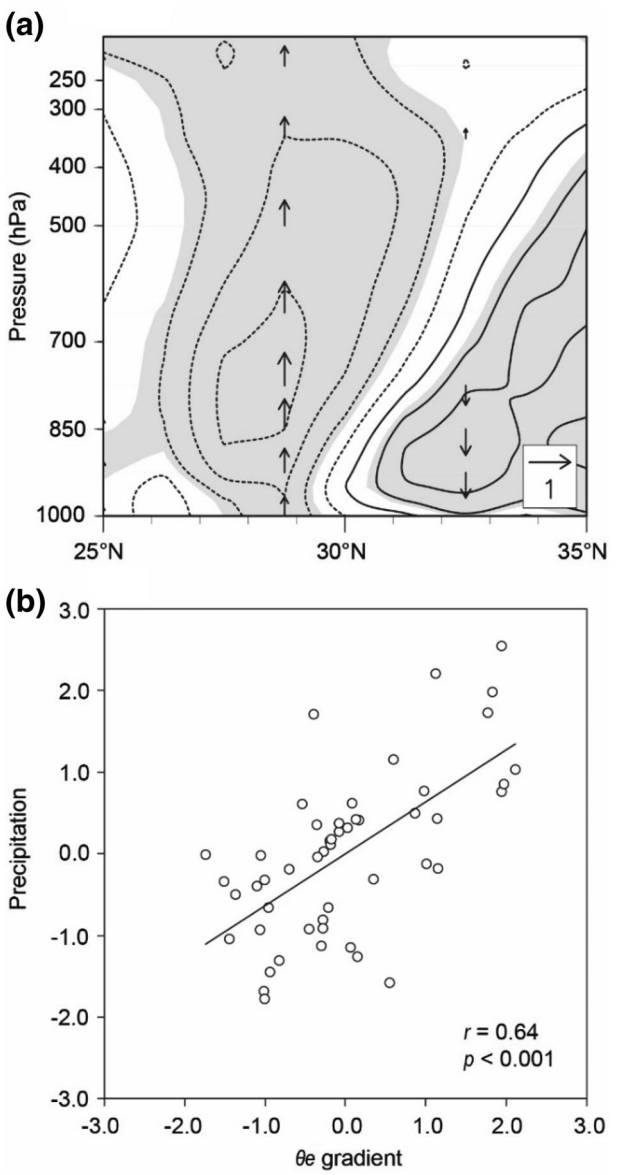

Fig. 3 **a** Correlation coefficients (contours) of the vertical velocity anomaly in the meridional–vertical cross section averaged over 106° E–119° E with the θe gradient ($-$ dθe/dy) anomaly over the YRB in summer. The contour interval is 0.2, and the zero contours are not shown. The shaded areas are significant with $p < 0.1$, and the arrows denote the vertical motion directions. **b** Relationship between the $-$ dθe/dy and precipitation over the YRB in summer during 1961–2010. All data are linearly detrended and standardized before the statistical calculations for the correlation analysis, and hereafter the same

intensity of the Meiyu front with a significant ($p < 0.001$) correlation coefficient of 0.64. This implies that the summer mean precipitation over the YRB highly depends on the intensity of the Meiyu front.

3.2 Summer EPEs over the YRB and their relationship with the Meiyu front

Besides the summer mean precipitation, the YRB EPEs mainly occur during the Meiyu period (Chen and Zhai 2015, 2016). Basically, EPEs are intense frontal precipitation processes, which are closely related to the strong upward movement of warm–wet air along a quasi-stationary front (Ninomiya and Shibagaki 2007). Figure 4a shows the frequency of summer EPEs. The distribution basically matches the standard deviation of summer precipitation (Fig. 1b). The high occurrences of those extreme events exist in the southern coastal region and the YRB. Specifically, over the

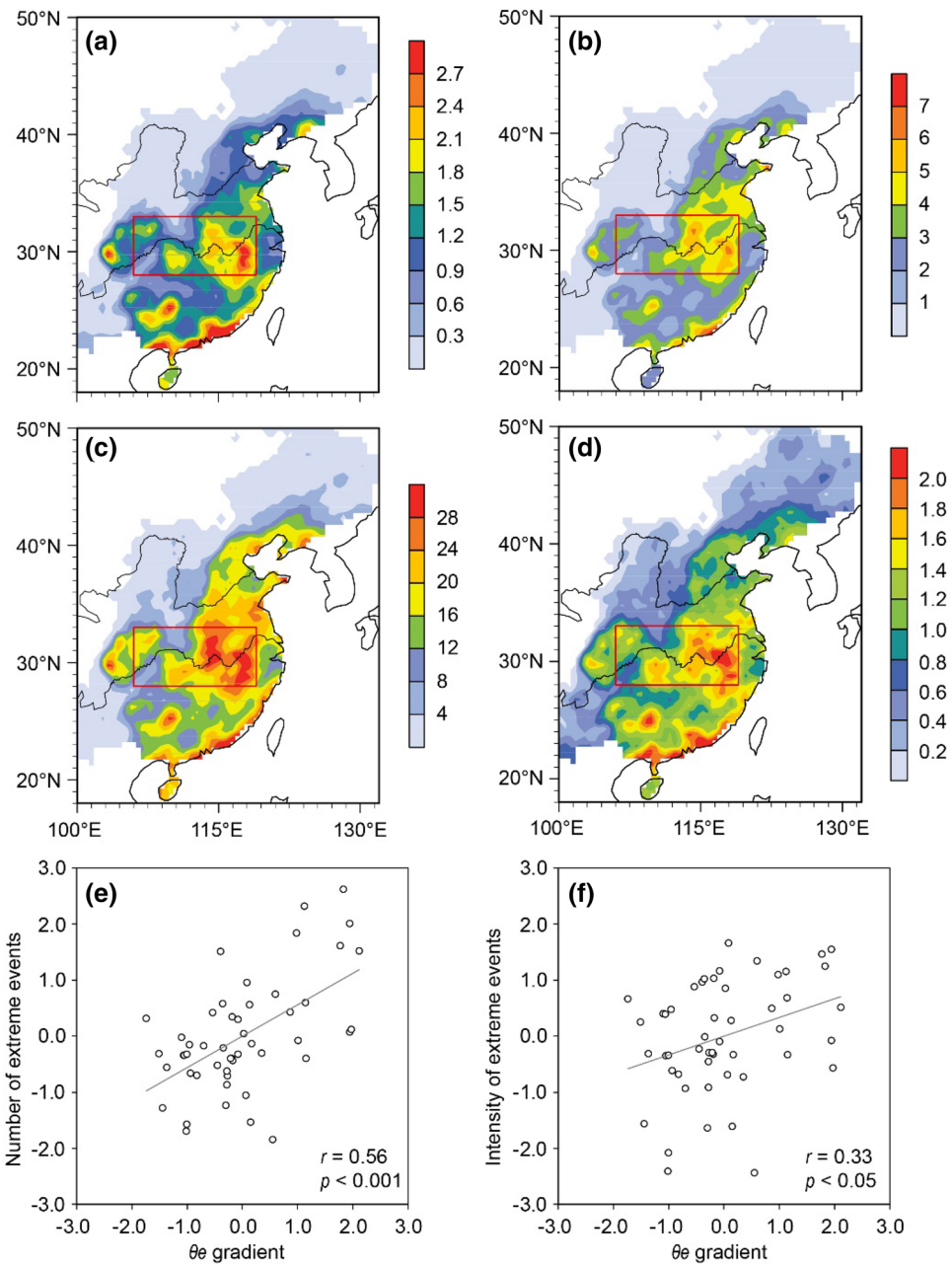

Fig. 4 **a** Climatology of the number of the summer extreme precipitation events (EPEs) during 1961–2010 (units: day). **b** The proportion of the summer EPEs in total rainy days in summer (units: %). **c** The proportion of the summer extreme precipitation amount in summer total precipitation (units: %). **d** Standard deviation of the summer EPEs during 1961–2010 (units: day). Relationships of meridional θe gradient ($-$ dθe/dy) with the (**e**) number and **f** intensity of the EPEs averaged over the YRB

YRB, the number of the EPEs accounts about 3–6% of the rainy days (days with precipitation over 1 mm; Fig. 4b), while the rainfall amount of those extreme events contributes to over 20% to about 30% of the total summer precipitation (Fig. 4c). This indicates that the EPEs are a large component of total summer precipitation over the YRB. Compared with the annual cycle of the YRB precipitation, the YRB EPEs tend to occur more frequently in summer (figure not shown): over half of the events (52%) happen in June to August. Similar to summer mean precipitation, the YRB is one of the large variability centers for the EPEs (Fig. 4d). As explained above, one can expect that this may be related to the Meiyu front intensity. We further illustrate the relationships between the EPEs and the θe gradient over the YRB. Indeed, both the number and intensity of the extreme events bear significantly positive correlations with the mean intensity of the Meiyu front, which are 0.56 ($p < 0.001$) and 0.33 ($p < 0.05$) for the past 5 decades, respectively (Fig. 4e, f).

In order to confirm the atmospheric backgrounds favorable for the YRB EPEs, Fig. 5 shows the correlations of the wind, θe, and $-$ dθe/dy anomalies with the anomalies of EPEs averaged over the YRB in summer. In

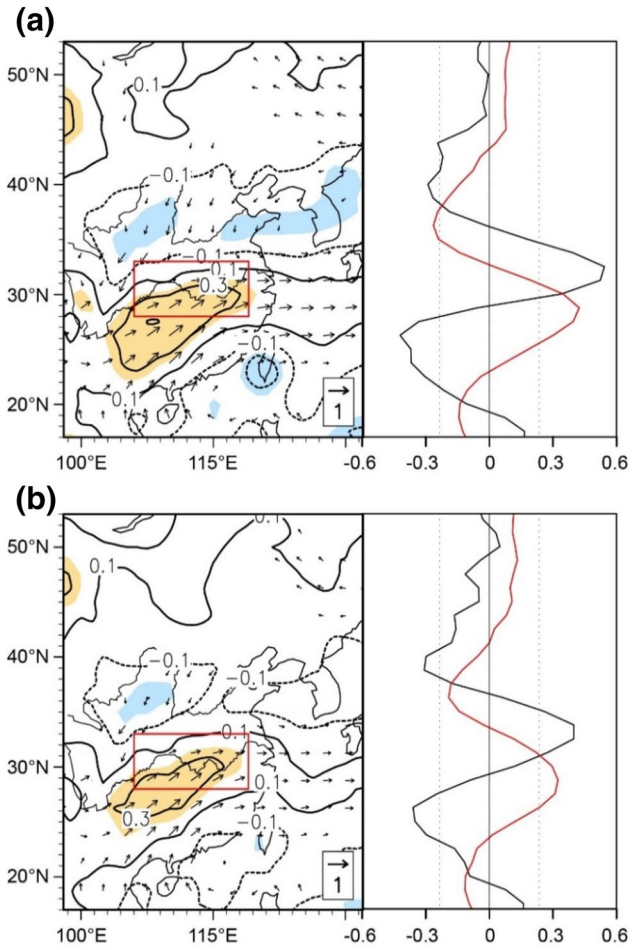

Fig. 5 **a** Correlation coefficients of 700 hPa θe (contours, the shaded areas are significant with $p<0.1$) and wind (arrows, only arrows significant with $p<0.1$ are shown) anomalies with the number of the EPEs averaged over the YRB in summer during 1961–2010. The right-hand panel shows the corresponding meridional correlation coefficients of θe (red line) and $-$ dθe/dy (black line) averaged over 106°–119° E with the number of the summer YRB EPEs, and the dotted straight lines denote the values significant with $p<0.1$. **b** Same as in **a**, but for the correlation coefficients with the intensity of the EPEs

the summer with more and stronger extreme events, an abnormally stronger southwesterly wind at the lower troposphere controls the southern China (Fig. 5a, b), leading to an excessive water vapor transported over the southern China to the YRB (figure not shown). On the one hand, more moisture converges over the YRB, which benefits the EPEs. On the other hand, the Meiyu front is enhanced associated with a higher θe over the south of the YRB (right panels of Fig. 5), resulting in a stronger ascending motion over the YRB (figure not shown), which is also favorable for the occurrence of the EPEs.

4 Effects of the ICP soil moisture

4.1 Relationship between the Meiyu front and the ICP soil moisture anomalies

Our recent study (Gao et al. 2019) revealed that the ICP spring soil moisture may influence the Asian summer monsoonal circulation via affecting local surface heating. This may potentially influence both the Meiyu front and the summer EPEs over the YRB. Here we firstly examine the relationship between the Meiyu front intensity and the spring soil moisture anomaly. Figure 6 shows the correlation of the spring soil moisture anomalies over the East Asian monsoon region with the summer θe gradient averaged over the YRB. A large area covered with negative correlations dominates the ICP (Fig. 6a). Furthermore, the anomaly phases of spring mean soil moisture averaged over the ICP (96° E–108° E and 10° N–25° N) and the summer Meiyu front intensity are generally opposite with a correlation coefficient of $-$ 0.36 ($p<0.01$; Fig. 6b). We also note that there exit weak upward trends in both variables during the study period, and thus the results with detrended data are further shown in Fig. 6c. Their relationship is even stronger with a correlation coefficient of $-$ 0.38. In other words, when the ICP land surface is abnormally drier in spring, the Meiyu front in the following summer is usually intensified, and vice versa. This means that soil moisture over the ICP in the preceding spring exists evident effects on the Meiyu front and thus influences the summer EPEs over the YRB. To verify the uncertainty of the GLDAS soil moisture, we compare the spring ICP soil moisture anomaly in GLDAS dataset with that in ERA-interim dataset for a shorter period of 1979–2010. The result show that the ICP soil moisture anomalies in two datasets are highly in agreement with each other by a correlation coefficient of 0.83 ($p<0.001$, figure not shown), which confirms that the GLDAS soil moisture is reliable in reflecting the actual dry–wet land surface states over the ICP. In the following analyses, the results are multiplied by $-$ 1 in order to make the corresponding soil moisture anomaly favorable for the Meiyu front enhancement.

4.2 Effects of the ICP soil moisture anomaly on the local thermal condition and monsoonal circulation

In this section, our analyses suggest that the abnormal surface heating induced by the soil moisture anomalies over the ICP would contribute to the west–east shifts of the WPSH. The resultant abnormal monsoonal wind affects the Meiyu front and thus the EPEs in summer. First of all, the scientific basis for the seasonal predictions of weather and climate anomalies by soil moisture is the strong persistence

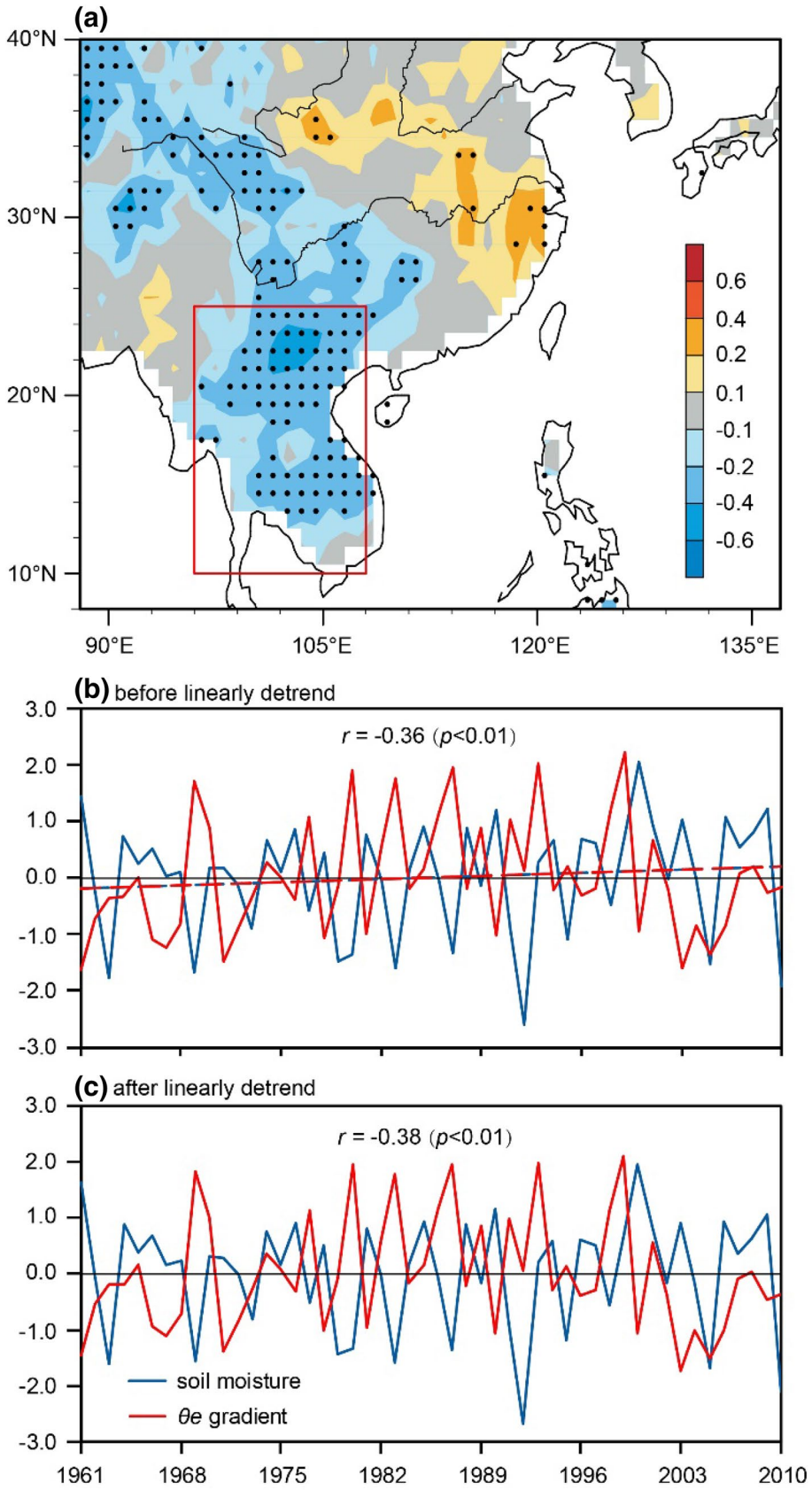

Fig. 6 **a** Correlation coefficients of spring soil moisture anomaly with the summer $-\mathrm{d}\theta e/\mathrm{d}y$ averaged over the YRB for the period of 1961–2010. The dotted areas are significant with $p < 0.1$. **b** The standardized spring soil moisture anomaly averaged over the ICP and summer $-\mathrm{d}\theta e/\mathrm{d}y$ anomaly averaged over the YRB. The dashed straight lines are their trend lines. **c** Same as in **b**, but for the linearly detrended anomalies

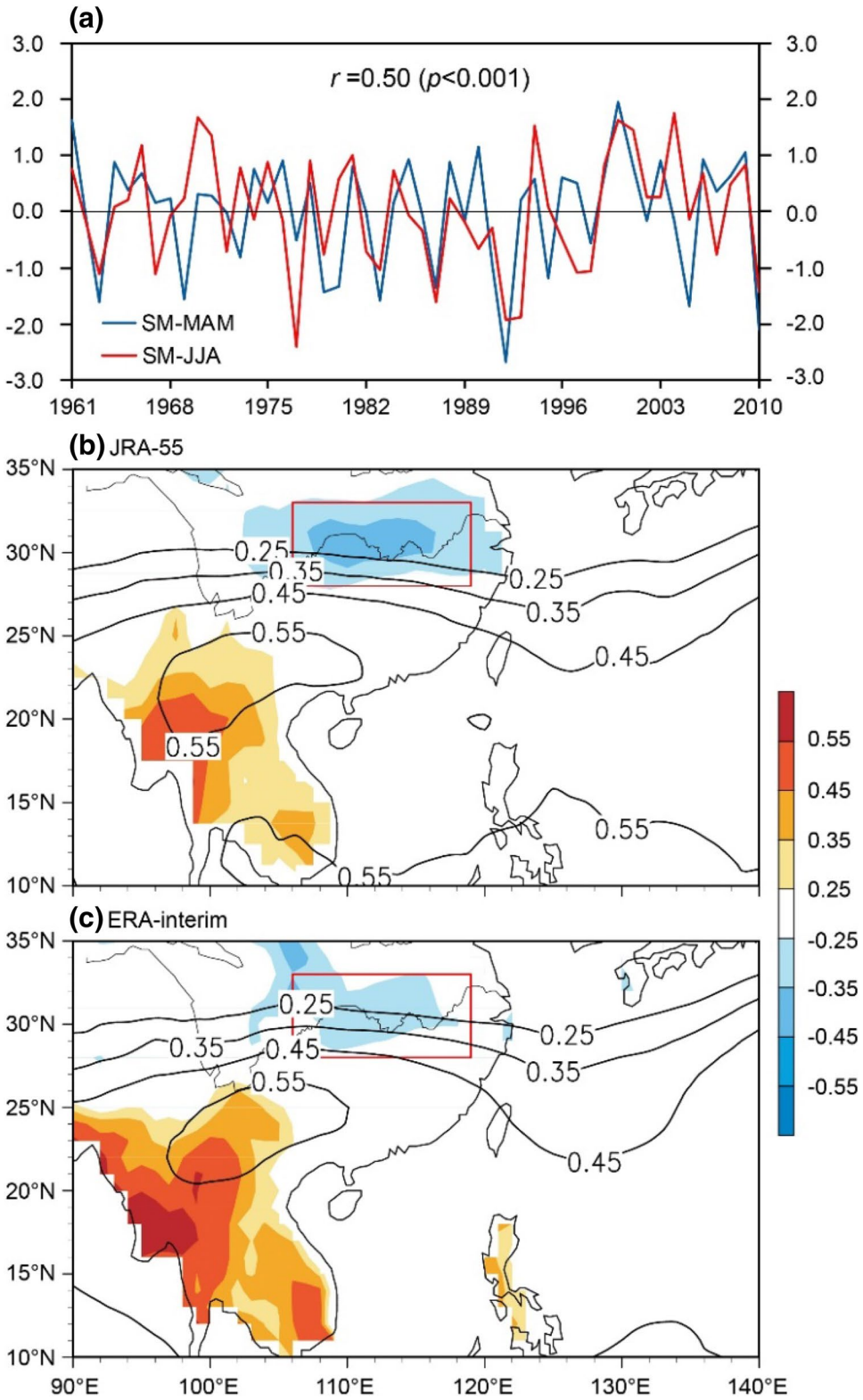

Fig. 7 **a** The standardized soil moisture anomaly in spring (SM-MAM) and summer (SM-JJA) averaged over the ICP. **b** Correlation coefficients of summer surface temperature (colors) and 500 hPa geopotential height anomalies (contours) with the negative spring ICP soil moisture anomaly for the period of 1961–2010. The absolute value of 0.25 are significant with $p < 0.1$. **c** Same as in **b**, but for the period of 1979–2010, and the surface temperature and geopotential height data from the JRA-55 are replaced by the ERA-interim dataset for comparison. The absolute value of 0.3 are significant with $p < 0.1$

(memory) of its abnormal states (Koster and Suarez 2001; Seneviratne et al. 2006; Dirmeyer et al. 2009). Thus, Fig. 7a illustrates the inter-annual anomalies of soil moisture in spring and the following summer averaged over the ICP. It is apparent that the soil moisture anomaly in spring can sustain in summer reflected by a significantly ($p < 0.001$) positive autocorrelation coefficient of 0.50. According to the results of Gao et al. (2019), the ICP soil moisture in spring

controls the local evapotranspiration, affecting the surface thermal condition until summer. For example, a drier soil condition over the ICP leads to a weaker evapotranspiration, increasing the surface temperature. The resultant abnormal thermal condition can further adjust the local geopotential height (Fischer et al. 2007). As shown in Fig. 7b, summer surface temperature is evidently affected by spring soil moisture anomaly over the ICP, which can be reflected by a strong correlation between their anomalies over there. The correlation coefficient of summer geopotential height at 500 hPa level with negative spring soil moisture anomaly over the ICP also demonstrates a relatively lager positive value over there. This confirms that the abnormal heating induced by a lower soil moisture uplifts the local geopotential height. Besides, the results are very similar when the temperature and geopotential height data from JRA-55 are replaced by the ERA-interim data for the period of 1979–2010.

The local geopotential height anomaly associated with an abnormal heating over the ICP may bring additional effects on the westward extension of the WPSH. To clarify our assumption of such changes in the summer WPSH, we selected five driest years (1963, 1983, 1992, 2005, and 2010) and five wettest years (1961, 1964, 1990, 2000, and 2009) according to spring soil moisture anomaly over the ICP, respectively, for the composite analysis. In the dry cases, the mean air temperature in summer over the ICP is abnormally

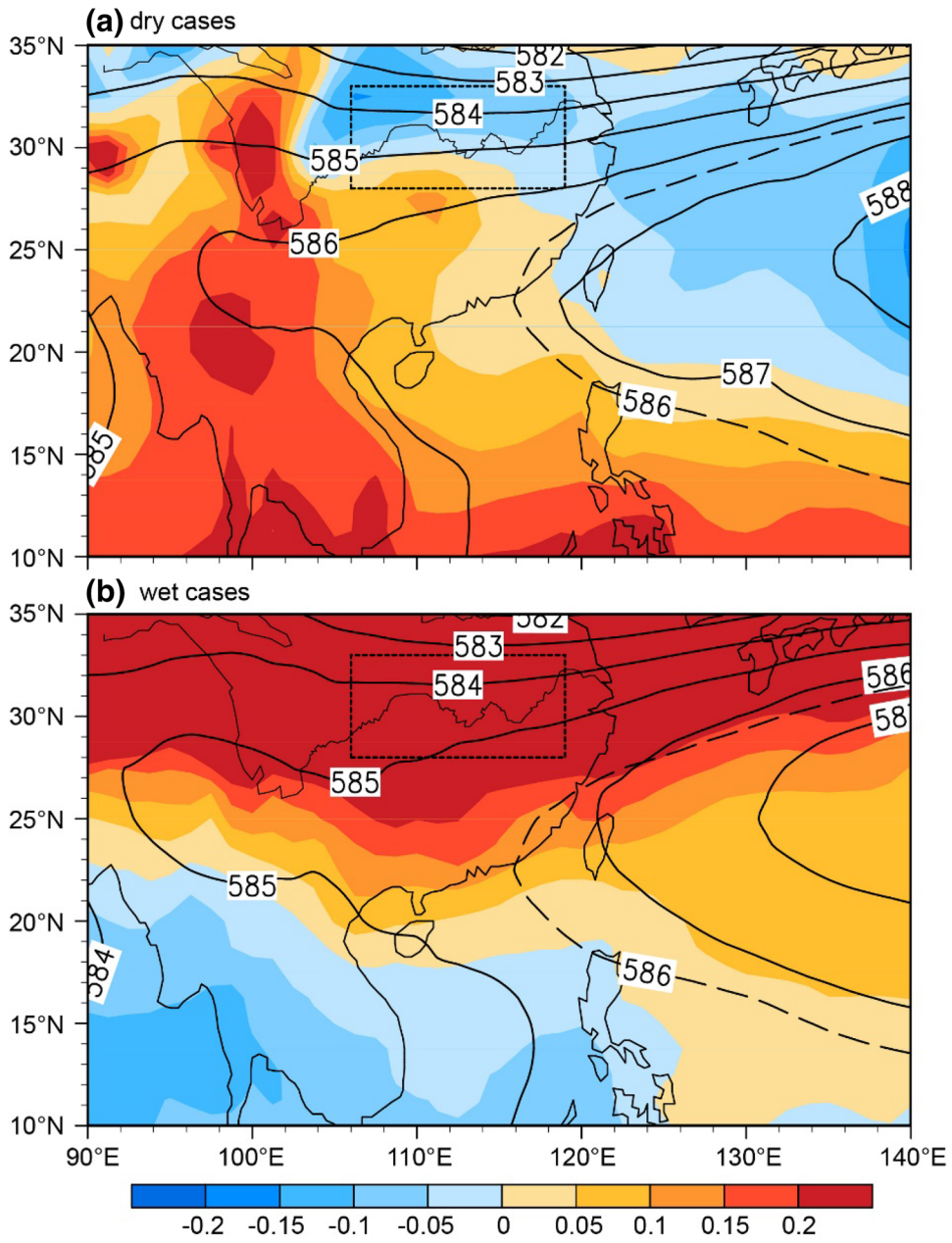

Fig. 8 Composite anomalies of 500 hPa geopotential height (contours, units: dagpm) and air temperature (colors, averaged from 300 to 1000 hPa) in summer for the **a** dry ICP cases and **b** wet ICP cases. Dashed lines are the climatology of 586 dagpm contour in summer for the period of 1961–2010

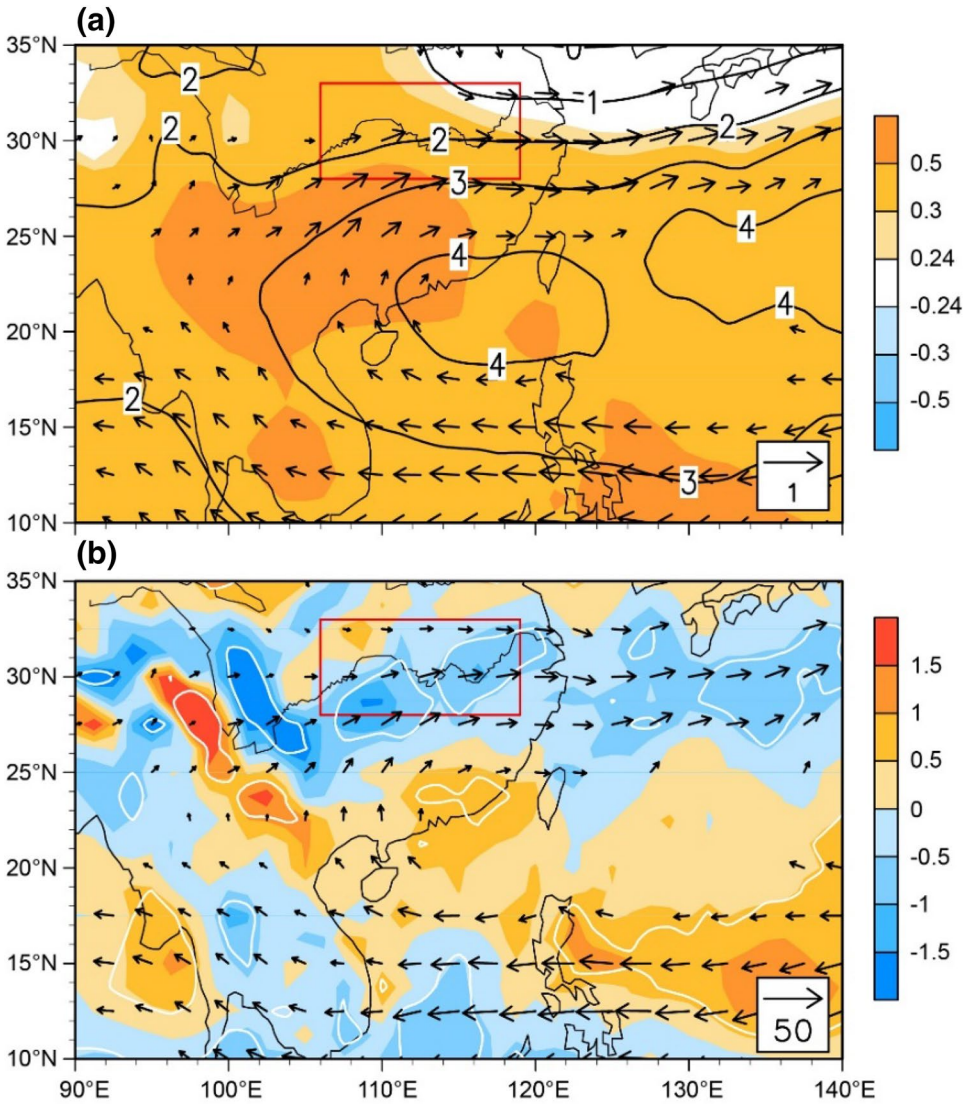

Fig. 9 **a** Regression of summer 700 hPa wind (arrows, units: m s^{-1}) and geopotential height (contours, units: gpm) anomalies with respect to the negative standardized spring soil moisture over the ICP for the period of 1961–2010. The shaded colors denote the correlation coefficients between the summer geopotential height and the negative spring ICP soil moisture anomaly. The shown arrows and shaded areas are significant with $p < 0.1$. **b** Regression of summer water vapor flux (arrows, units: kg m^{-1} s^{-1}) and its divergence (colors, units: $1e^{-5}$ kg m^{-2} s^{-1}) anomalies integrated from 300 to 1000 hPa with respect to the negative standardized spring soil moisture over the ICP for the period of 1961–2010. The shown arrows and the areas within white lines are significant with $p < 0.1$. All data are linearly detrended before the statistical calculations for the regression analysis, and hereafter the same

higher by over 0.15 K, and the WPSH extends westward dramatically (Fig. 8a). On the other hand, in the wet cases, the summer air temperature over the ICP decreases, and the WPSH retreats eastward (Fig. 8b). Such anomaly phases verify that the local geopotential height anomaly induced by the abnormal ICP soil moisture would attract/hamper the westward extension of the WPSH, which is a key component of the East Asian summer monsoon system.

To further investigate the responses of the East Asian summer monsoonal circulations, the anomalies of 700 hPa wind, geopotential height, and tropospheric moisture flux fields in summer related to the spring soil moisture anomalies over the ICP are shown in Fig. 9. The abnormal center of the 700 hPa geopotential height with 4 gpm is located in the western Pacific Ocean near the southern coastal line of China and extents towards the ICP land (Fig. 9a). Correspondingly, an anomalous anticyclone wind field exists along the west rim of the abnormal geopotential height center, resulting in an enhanced southwesterly wind over the Southern China. Such a wind anomaly at lower troposphere plays a key role in variations of the air moisture transport. Thus, the abnormally stronger southwesterly wind brings more water vapor to the YRB (Fig. 9b), leading to an evidently excessive moisture converging over there.

The enhancement of the warm and wet air transporting to the YRB provides sufficient water sources for the local summer precipitation. Meanwhile, the Meiyu front is also affected by this anomalous water vapor flux. As reflected in Fig. 10, associated with the abnormal wind field, the θe in the south is abnormally higher, and the meridional θe gradient across the YRB is relatively larger than normal. This suggests that the Meiyu front is intensified with more warm and wet air flow over the Southern China, which is induced by the abnormally drier soil over the ICP. Furthermore, accompanied by an enhanced Meiyu front, the ascending motion above the YRB is intensified as well (Fig. 11),

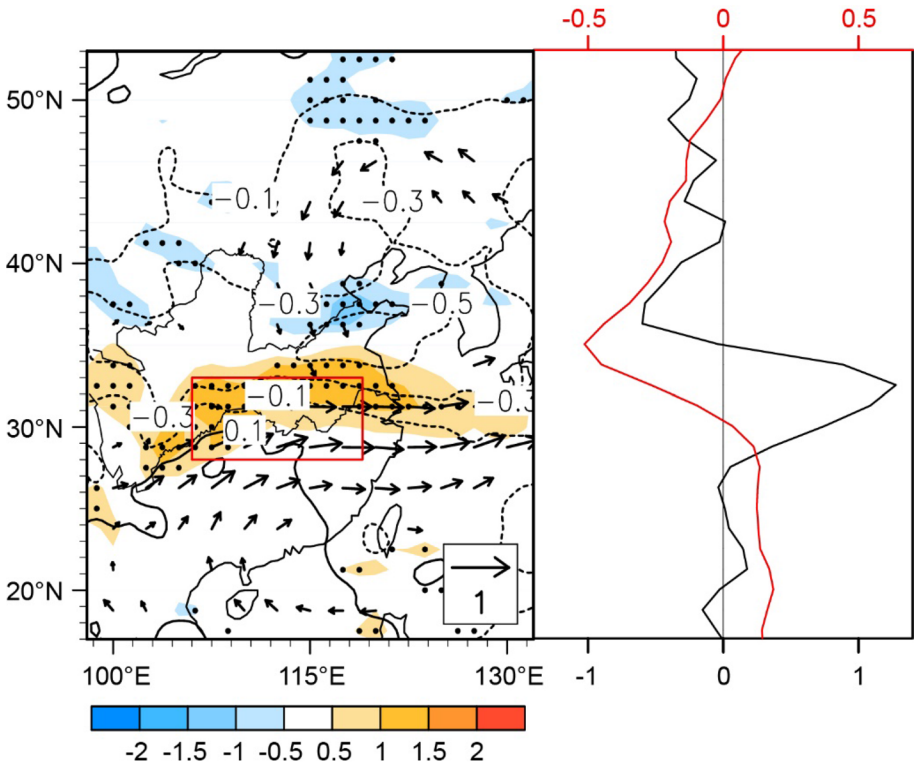

Fig. 10 Regressions of the 700 hPa summer θe (contours, units: K), wind (arrows, units: m s^{-1}) and − dθe/dy (colors, units: 1e−6 K m^{-1}) anomalies with respect to the negative standardized spring soil moisture over the ICP for the period of 1961–2010. The colored areas with dots are significant with $p < 0.1$. The wind anomalies significant with $p < 0.1$ are shown for comparison. The right-hand panel shows the corresponding meridional θe (red line) and − dθe/dy (black line) anomalies averaged over 106° E–119° E

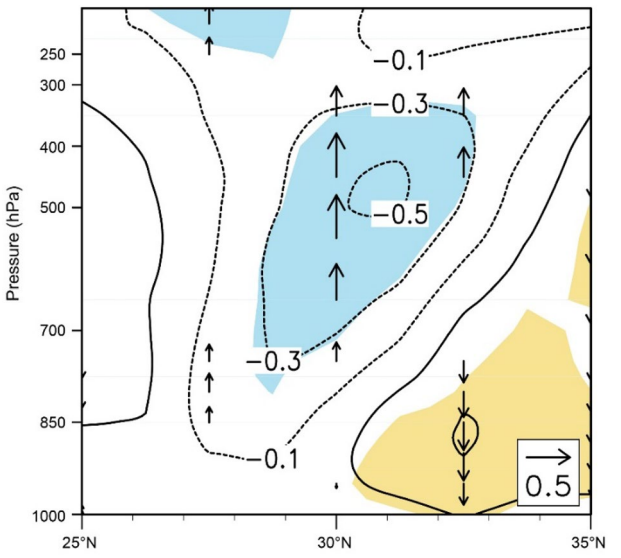

Fig. 11 Regression of the vertical velocity anomaly (contours, units: 1e^{-2} Pa s^{-1}) in the meridional–vertical cross section averaged over 106° E–119° E with respect to the negative standardized spring soil moisture over the ICP for the period of 1961–2010. The shaded areas are significant with $p < 0.1$. The arrows denote the vertical motion directions

which implies a favorable condition for intense precipitation in summer. Therefore, the intensity and frequency of summer EPEs over the YRB may increase.

In addition, we adopt the omega equation to diagnosis the maintenance mechanisms of the abnormal ascending motion. According to this equation, in the case of neglecting the diabatic heating, the vertical gradient of absolute vorticity advection (term B) and the temperature advection (term C) are two major contributions to the vertical motion (term A). Firstly, the ascending motion (positive term A) responding to the lower ICP soil moisture mainly dominates the YRB (Fig. 12a), which also implies that the summer with more and stronger convective activities over the YRB usually exists after a drier spring over the ICP land. Figure 12b, c further illustrate the responses of term B and term C in Eq. (2). It is evident that the ascent over the YRB is mainly maintained by term C, while the response of the term B is much weaker. Therefore, the abnormal warm temperature advection induced by the abnormally lower ICP soil moisture plays a major role in maintaining the upward motion anomaly over the YRB. This further confirms that the spring ICP soil moisture anomaly could affect the Meiyu front and the YRB EPEs by influencing the East Asian summer monsoonal circulation.

4.3 Response of summer EPEs to the spring ICP soil moisture anomaly

The aforementioned findings highlight the linkage between the Meiyu front and the EPEs in summer over the YRB and

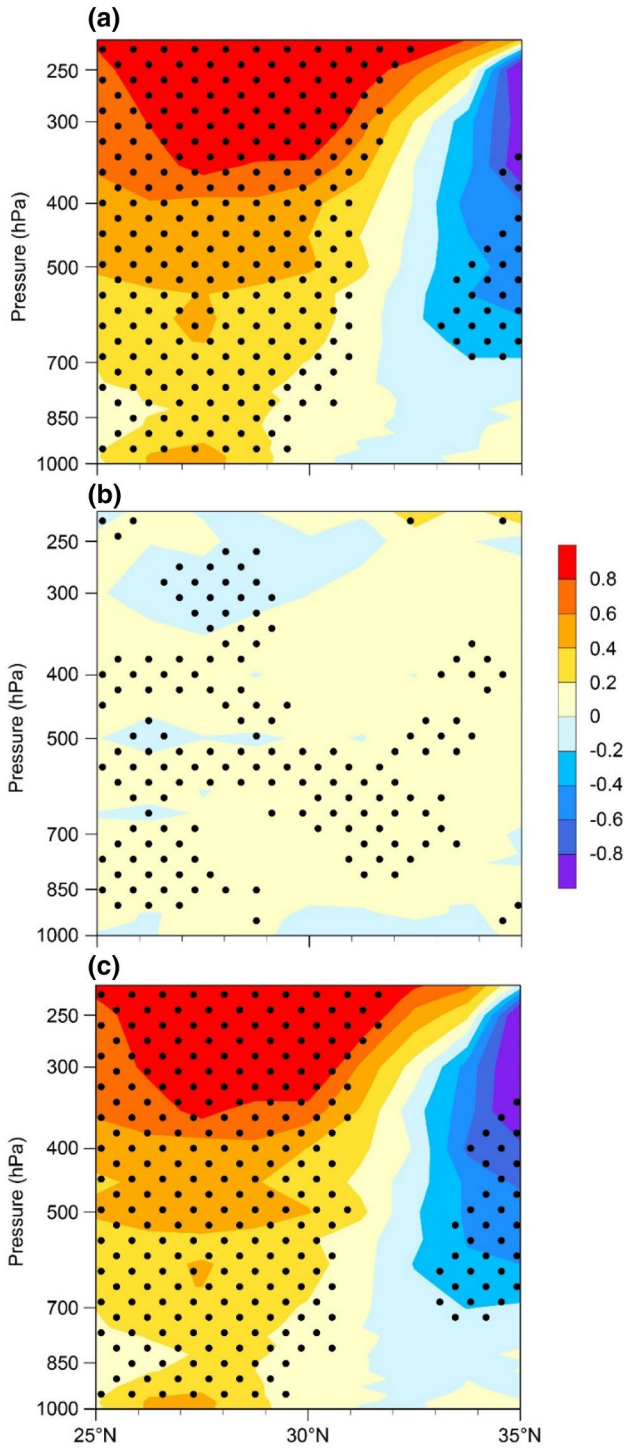

Fig. 12 Regression of the **a** term A, **b** term B, and **c** term C anomalies (units: $1e^{-16}$ m s^{-1} kg^{-1}) in the omega equation averaged over 106°–119° E with respect to the negative standardized spring soil moisture over the ICP for the period of 1961–2010. The dotted areas are significant with $p < 0.1$

also indicate that the Meiyu front is evidently affected by the spring ICP soil moisture anomaly. Therefore, it is expected to be a close relationship between the anomalies of the YRB EPEs in summer and the ICP soil moisture in spring. Indeed, the number and intensity of the summer EPEs averaged over the YRB bear negative correlations with the spring ICP soil moisture anomaly by the correlation coefficients of −0.41 and −0.40 for the 5 decades (Fig. 13), which are both significant with $p < 0.01$. In other words, when the ICP soil is abnormally drier in spring, both the frequency and intensity of EPEs over the YRB generally rise during the following summer, and vice versa. Based on the regression approach, about 16% of the changes in summer EPEs over the YRB can be attributed to spring soil moisture anomaly over the ICP.

To clarify our findings, the Fig. 14 further demonstrates the spatial distribution of responses of the EPEs to the ICP soil moisture anomalies. Generally speaking, the responses of summer EPEs to the negative ICP soil moisture anomalies are mostly evident over the YRB with large amount of significantly ($p < 0.1$) positive values (Fig. 14a, b). Considering that the abnormal atmospheric circulation in summer might be related to the El Niño/Southern Oscillation (ENSO) events. ENSO is the most prominent climate variability in the tropical Pacific, and its SST anomaly reaches the peak in boreal winter (December, January, and February). Thus, ENSO SST anomaly usually undergoes its developing and decaying stages in the preceding and following summers, respectively. They can cause evident climatic effects on Asia (Xie et al. 2009; Wen et al. 2018). Here, the previous and subsequent winter SST anomalies over the Niño 3.4 region (5° N–5° S and 120° W–170° W) are calculated as the ENSO decaying and developing signals. Figure 14c–f demonstrate the results after removing these signals, which are highly consistent with the results in Fig. 14a, b. Moreover, the Indian Ocean basin (20° N–20° S and 40° W–100° W) SST anomaly (Indian Ocean basin mode, IOBM) associated with the ENSO events is usually strong in summer, sustaining the effects of ENSO forcing on the monsoonal circulation (Tao et al. 2016; Xie et al. 2016). We additionally show the results after removing the IOBM signal in Fig. 14g, h. Likewise, there are still strong responses of summer EPEs over the YRB to the abnormal spring ICP soil moisture in both frequency and intensity. This suggests that the effect of the spring ICP soil moisture on the summer YRB EPEs is largely independent of tropical SST forcing.

5 Summary and discussion

Extreme precipitation exerts a great impact on the human life and has attracted extensive attention in the field of climate research. In this study, we firstly demonstrate the relationship between the summer EREs over the YRB and the Meiyu front. Results show that the summer EPEs exhibit large variabilities over the YRB, and they are highly related to the mean states of the Meiyu front. Both the frequency and intensity of the YRB EPEs increase with a relatively stronger Meiyu front in summer. Further analyses suggest that the Meiyu front variations are significantly correlated with the preceding spring soil moisture anomalies over the ICP. When the ICP soil is anomalously drier in spring, the Meiyu front is enhanced in summer characterized by an abnormally stronger meridional θe gradient over the YRB, and vice versa.

The soil moisture anomaly over the ICP could evidently affect local surface thermal condition through the evapotranspiration process. Thus, the local temperature is abnormally higher associated with a drier ICP soil. Due to the slow-varying ability, the ICP soil moisture anomaly and its local thermal effect in spring could sustain to summer. Then, this abnormally stronger surface heating leads to an uplifted local summer geopotential height. This contributes to the WPSH extending westward, which is a key process in the East Asian summer monsoon variations. Consequently, the southwesterly monsoonal wind over the southern China is abnormally intensified, bringing more water vapor to the YRB. Meanwhile, the redundant warm–wet air conveyed to the YRB increases the local meridional θe gradient, which indicates an enhancement of the Meiyu front and a favorable condition for the ascending motion. The diagnosis of the omega equation suggests that the ascent over the YRB is mainly attributed to the warm temperature advection. This further verifies that the abnormal warm and moist flow with the monsoonal circulation anomaly induced by the lower ICP soil moisture provides a favorable condition for the upward movement in summer over the YRB. An abundant moisture transporting and a favorable condition for convective activities are both beneficial to intense precipitation. Therefore, more and stronger EPEs occur in summer over the YRB with a drier surface condition in spring over the ICP. On the other hand, the risk of summer EPEs reduces when the spring ICP soil moisture is abnormally higher.

Generally, the primary driving factor of soil moisture anomaly is precipitation, and EPSs are also closely linked to local precipitation. Using the CRU dataset, we calculate the spring precipitation and summer precipitation averaged over the ICP and the YRB, respectively. A strong negative relationship between their anomalies exists for the period of 1961–2018 by a significant ($p < 0.05$) correlation coefficient of -0.26 (figure not shown). This situation hints that our findings are still robust for the period including the recent 8 years.

Understanding the nature and causes of summer EPEs over East Asia has always been a great challenge. Our study emphasizes the non-local effects of the spring ICP soil moisture on the East Asia climate extremes, and provides a seasonal predictor of the YRB EPEs in summer. The potential benefits of improved seasonal prediction are enormous for hundreds of millions of people living over the YRB.

Fig. 14 Regression of the **a** number (units: day) and **b** intensity (units: mm day^{-1}) of the summer EPEs with respect to the negative standardized spring soil moisture over the ICP for the period of 1961–2010. Same as in **a** and **b**, but for the results after removing the parts in soil moisture anomaly linearly related to the (**c**, **d**) ENSO decaying, **e**, **f** developing, and **g**, **h** IOBM signals. The dotted areas are significant with $p < 0.1$

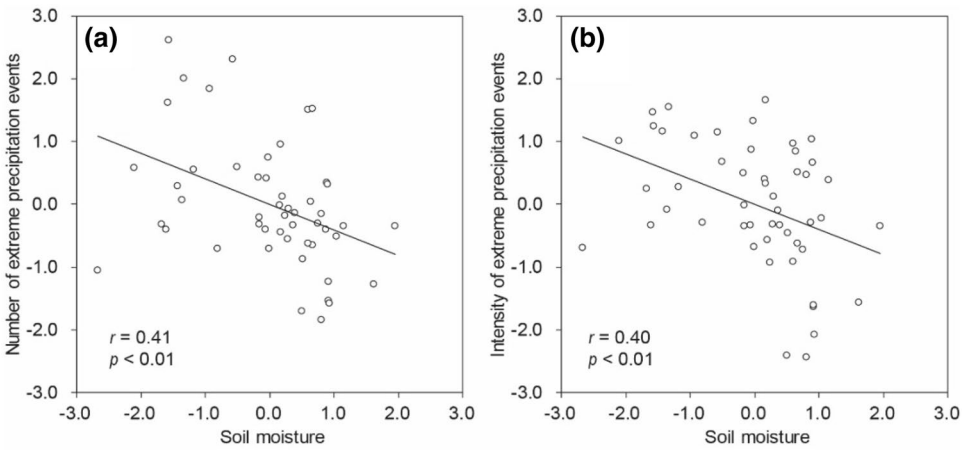

Fig. 13 Relationships of the spring soil moisture anomaly averaged over the ICP with the **a** number and **b** intensity of the summer EPEs averaged over the YRB

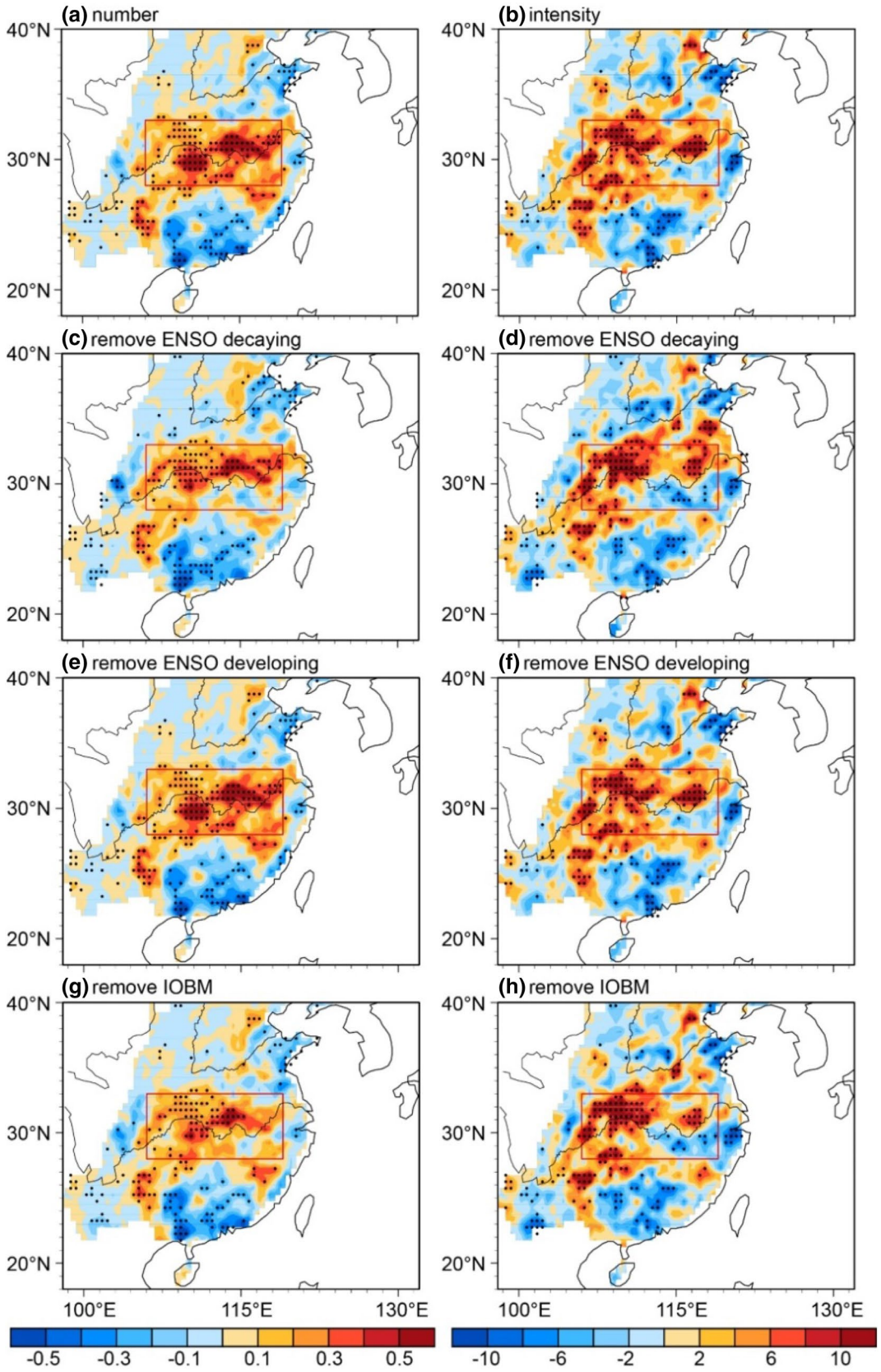
(a) number
(b) intensity
(c) remove ENSO decaying
(d) remove ENSO decaying
(e) remove ENSO developing
(f) remove ENSO developing
(g) remove IOBM
(h) remove IOBM
40°N
30°N
20°N
100°E
115°E
130°E
-0.5
-0.3
-0.1
0.1
0.3
0.5
-10
-6
-2
2
6
10

Acknowledgements This work was supported by the Fundamental Research Funds for the Central Universities (2018B03114 and 2019B18814), the Natural Science Foundation of China (41831175, 41905054, and 41861144013), and the China Postdoctoral Science Foundation (2019M651665).

References

Bellucci A, Haarsma R, Bellouin N, Booth B, Cagnazzo C, van den Hurk B, Keenlyside N, Koenigk T, Massonnet F, Materia S, Weiss M (2015) Advancements in decadal climate predictability: the role of nonoceanic drivers. Rev Geophys 53:165–202

Cen S, Gong Y, Lai X, Peng L (2015) The relationship between the atmospheric heating source/sink anomalies of Asian monsoon and flood/drought in the Yangtze River basin in the Meiyu period. J Trop Meteorol 21:352–360

Chen J, Chen L (1991) Influence of ocean–continent distribution in the south part of Asia on the formation of Asian summer monsoon. J Appl Meterol Sci 2:355–361 (**in Chinese**)

Chen Y, Zhai P (2013) Persistent extreme precipitation events in China during 1951–2010. Clim Res 57:143–155

Chen Y, Zhai P (2015) Synoptic-scale precursors of the East Asia/Pacific teleconnection pattern responsible for persistent extreme precipitation in the Yangtze River Valley. Q J R Meteorol Soc 141:1389–1403

Chen Y, Zhai P (2016) Mechanisms for concurrent low-latitude circulation anomalies responsible for persistent extreme precipitation in the Yangtze River Valley. Clim Dyn 47:989–1006

Cheng SJ, Huang JP (2016) Enhanced soil moisture drying in transitional regions under a warming climate. J Geophys Res Atmos 121:2542–2555

Cheng SJ, Guan XD, Huang JP, Ji F, Guo RX (2015) Long-term trend and variability of soil moisture over East Asia. J Geophys Res Atmos 120:8658–8670

Ding YH (1992) Summer monsoon rainfall in China. J Meteorol Soc Jpn 70:373–396

Ding Y, Chan JCL (2005) The East Asian summer monsoon: an overview. Meteorol Atmos Phys 89:117–142

Ding Y, Liu J, Sun Y, Liu Y, He J, Song Y (2007) A study of the synoptic-climatology of the Meiyu system in East Asia. Chin J Atmos Sci 31:1082–1101 (**in Chinese**)

Dirmeyer PA (2011) The terrestrial segment of soil moisture–climate coupling. Geophys Res Lett 38:L16702

Dirmeyer PA, Schlosser CA, Brubaker KL (2009) Precipitation, recycling, and land memory: an integrated analysis. J Hydrometeorol 10:278–288

Douville H (2002) Influence of soil moisture on the Asian and African monsoons. Part II: interannual variability. J Clim 15:701–720

Douville H, Chauvin F, Broqua H (2001) Influence of soil moisture on the Asian and African monsoons. Part I: mean monsoon and daily precipitation. J Clim 14:2381–2403

Ek MB, Mitchell KE, Lin Y, Rogers E, Grunmann P, Koren V, Gayno G, Tarpley JD (2003) Implementation of Noah land surface model advances in the National Centers for Environmental Prediction operational mesoscale Eta model. J Geophys Res Atmos 108:8851

Feng L, Li T, Yu W (2014) Cause of severe droughts in Southwest China during 1951–2010. Clim Dyn 43:2033–2042

Fischer EM, Seneviratne SI, Vidale PL, Lüthi D, Schär C (2007) Soil moisture–atmosphere interactions during the 2003 European summer heat wave. J Clim 20:5081–5099

Gao C, Chen H, Sun S, Xu B, Ongoma V, Zhu S, Ma H, Li X (2018) Regional features and seasonality of land–atmosphere coupling over eastern China. Adv Atmos Sci 35:689–701

Gao C, Chen H, Li G, Ma H, Li X, Long S, Xu B, Li X, Zeng X, Yan H, Wang Z, Yang S (2019) Land–atmosphere interaction over the Indo-China Peninsula during spring and its effect on the following summer climate over the Yangtze River basin. Clim Dyn 53:6181–6198

Guan Z, Han J, Li M (2011) Circulation patterns of regional mean daily precipitation extremes over the middle and lower reaches of the Yangtze River during the boreal summer. Clim Res 50:171–185

He J, Ju J, Wen Z, Lü J, Jin Q (2007) A review of recent advances in research on Asian monsoon in China. Adv Atmos Sci 24:972–992

Holton JR (2004) An introduction to dynamic meterology, 4th edn. Elsevier Academic Press, Burlington

Hsu HH, Liu X (2003) Relationship between the Tibetan Plateau heating and East Asian summer monsoon rainfall. Geophys Res Lett 30:1182–1200

Huang R, Xu Y, Wang P, Zhou L (1998) The features of the catastrophic flood over the Changjiang river basin during the summer of 1998 and cause exploration. Clim Environ Res 3:300–313 (**in Chinese**)

Huang R, Zhou L, Chen W (2003) The progresses of recent studies on the variabilities of the East Asian monsoon and their causes. Adv Atmos Sci 20:55–69

Huang J, Yu H, Guan X, Wang G, Guo R (2015) Accelerated dryland expansion under climate change. Nat Clim Change 6:166–171

Huang J, Ji M, Xie Y, Wang S, He Y, Ran J (2016) Global semi-arid climate change over last 60 years. Clim Dyn 46:1131–1150

Huang J, Li Y, Fu C, Chen F, Fu Q, Dai A, Shinoda M, Ma Z, Guo W, Li Z, Zhang L, Liu Y, Yu H, He Y, Xie Y, Guan X, Ji M, Lin L, Wang S, Yan H, Wang G (2017) Dryland climate change: recent progress and challenges. Rev Geophys 55:719–778

Jiang T, Kundzewicz ZW, Su B (2010) Changes in monthly precipitation and flood hazard in the Yangtze River Basin, China. Int J Climatol 28:1471–1481

Jin Q, He J, Chen L, Zhu C (2006) Impacts of ocean–land distribution over the southern Asia and the continents over the southern Hemisphere on the formation of Asian summer monsoon circulation. Chin J Atmos Sci 30:1043–1053 (**in Chinese**)

Jin Q, He J, Chen L, Zhu C (2006) Impact of ocean–continent distribution over Southern Asia on the formation of summer monsoon. Acta Meteorol Sin 20:95–108

Kobayashi S, Ota Y, Harada Y, Ebita A, Moriya M, Onoda H, Onogi K, Kamahori H, Kobayashi C, Endo H, Miyaoka K, Takahashi K (2015) The JRA-55 reanalysis: general specifications and basic characteristics. J Meteorol Soc Jpn Ser II 93:5–48

Koster RD, Suarez MJ (2001) Soil moisture memory on climate models. J Hydrometeorol 2:558–570

Li X, Lu R (2017) Extratropical factors affecting the variability in summer precipitation over the Yangtze River basin, China. J Clim 30:8357–8374

Li X, Lu R (2018) Subseasonal change in the seesaw pattern of precipitation between the Yangtze River basin and the tropical Western North Pacific during summer. Adv Atmos Sci 35:1231–1242

Liang L, Chen H (2010) Possible linkage between spring soil moisture anomalies over South China and summer rainfall in China. Trans Atmos Sci 33:536–546 (**in Chinese**)

Liu L, Zhang R, Zuo Z (2017) Effect of spring precipitation on summer precipitation in eastern China: role of soil moisture. J Clim 30:9183–9194

Lu R (2004) Associations among the components of the East Asian summer monsoon system in the meridional direction. J Meteorol Soc Jpn 82:155–165

Luo Y, Chen Y (2015) Investigation of the predictability and physical mechanisms of an extreme-rainfall-producing mesoscale

convective system along the Meiyu front in East China: an ensemble approach. J Geophys Res Atmos 120:10593–510618

Ma J, Yang S, Wang Z (2018) Influence of spring soil moisture anomaly in the Indo-China peninsula on the establishment and development of Asian tropical summer monsoon. Meteorol Environ Sci 41:19–30 (**in Chinese**)

Meng L, Long D, Quiring SM, Shen Y (2014) Statistical analysis of the relationship between spring soil moisture and summer precipitation in East China. Int J Climatol 34:1511–1523

Ninomiya K, Shibagaki Y (2007) Multi-scale features of the Meiyu-Baiu front and associated precipitation systems. J Meteorol Soc Jpn B 85:103–122

Rayner NA, Parker DE, Horton EB, Folland CK, Alexander LV, Rowell DP (2003) Global analyses of sea surface temperature, sea ice, and night marine air temperature since the late nineteenth century. J Geophys Res 108:4407

Rodell M, Houser PR, Jambor U, Gottschalck J, Mitchell K, Meng CJ, Arsenault K, Cosgrove B, Radakovich J, Bosilovich M, Entin JK, Walker JP, Lohmann D, Toll D (2004) The global land data assimilation system. Bull Am Meteorol Soc 85:381–394

Sampe T, Xie S-P (2010) Large-scale dynamics of the Meiyu-Baiu rainband: environmental forcing by the westerly jet. J Clim 23:113–134

Seneviratne SI, Koster RD, Guo Z, Dirmeyer PA, Kowalczyk E, Lawrence D, Liu P, Lu C-H, Mocko D, Oleson KW, Verseghy D (2006) Soil moisture memory in AGCM simulations: analysis of Global Land-Atmosphere Coupling Experiment (GLACE) data. J Hydrometeorol 7:1090–1112

Seneviratne SI, Corti T, Davin EL, Hirschi M, Jaeger EB, Lehner I, Orlowsky B, Teuling AJ (2010) Investigating soil moisture–climate interactions in a changing climate: a review. Earth Sci Rev 99:125–161

Sheffield J, Goteti G, Wood EF (2006) Development of a 50-year high-resolution global dataset of meteorological forcings for land surface modeling. J Clim 19:3088–3111

Tao W, Huang G, Hu K, Gong H, Wen G, Liu L (2016) A study of biases in simulation of the Indian Ocean basin mode and its capacitor effect in CMIP3/CMIP5 models. Clim Dyn 46:205–226

Wang B, Linho (2002) Rainy season of the Asian-Pacific summer monsoon. J Clim 15:386–398

Wang Y, Yan Z (2011) Changes of frequency of summer precipitation extremes over the Yangtze River in association with large-scale oceanic-atmospheric conditions. Adv Atmos Sci 28:1118–1128

Wen Z, Wu N, Feng Y, Lin L, Yuan Z, Chen B (2007) A quantitative diagnosis for the mechanisms of spring droughts in South China. Chin J Atmos Sci 31:1223–1236 (**in Chinese**)

Wen N, Liu Z, Li L (2018) Direct ENSO impact on East Asian summer precipitation in the developing summer. Clim Dyn 52:6799–6815

Wu J, Gao X (2013) A gridded daily observation dataset over China region and comparison with the other datasets. Chin J Geophys 56:1102–1111 (**in Chinese**)

Wu L, Zhang J (2013) Asymmetric effects of soil moisture on mean daily maximum and minimum temperatures over eastern China. Meteorol Atmos Phys 122:199–213

Wu G, Liu Y, Zhang Q, Duan A, Wang T, Wan R, Liu X, Li W, Wang Z, Liang X (2007) The influence of mechanical and thermal forcing by the Tibetan Plateau on Asian climate. J Hydrometeorol 8:205–208

Xie S-P, Hu K, Hafner J, Tokinaga H, Du Y, Huang G, Sampe T (2009) Indian Ocean capacitor effect on Indo–Western Pacific climate during the summer following El Niño. J Clim 22:730–747

Xie S-P, Kosaka Y, Du Y, Hu K, Chowdary JS, Huang G (2016) Indo-Western Pacific Ocean capacitor and coherent climate anomalies in post-ENSO summer: a review. Adv Atmos Sci 33:411–432

Xu Y, Gao X, Yan S, Xu C, Ying S, Giorgi F (2009) A daily temperature dataset over China and its application in validating a RCM simulation. Adv Atmos Sci 26:763–772

Yang K, Zhang J, Wu L, Wei J (2019) Prediction of summer hot extremes over the middle and lower reaches of the Yangtze River valley. Clim Dyn 52:2943–2957

Zhai P, Zhang X, Hui W, Pan X (2005) Trends in total precipitation and frequency of daily precipitation extremes over China. J Clim 18:1096–1108

Zhan Y, Lin Z (2011) The relationship between June precipitation over mid-lower reaches of the Yangtze River basin and spring soil moisture over the East Asian monsoon region. Acta Meteorol Sin 25:355–363

Zhang Y, Qian Y (2002) Mechanism of thermal features over the Indo-China Peninsula and possible effects on the onset of the South China Sea monsoon. Adv Atmos Sci 19:885–900

Zhou Y, Deng G, Chen H, Chen Z (2005) Synoptic features of the second Meiyu period in 1998 over China. J Meteorol Res 19:31–43

Zuo Z, Zhang R (2007) The spring soil moisture and the summer rainfall in eastern China. Chin Sci Bull 52:3310–3312

Zuo Z, Zhang R (2016) Influence of soil moisture in eastern China on the East Asian summer monsoon. Adv Atmos Sci 33:151–163

Zuo Z, Song Y, Kumar A, Zhang R, Yan X, Jha B (2012) Role of thermal condition over Asia in the weakening Asian summer monsoon under global warming background. J Clim 25:3431–3436

Publisher's Note Springer Nature remains neutral with regard to jurisdictional claims in published maps and institutional affiliations.